AIAA Journal of Aircraft (2021), Vol. 58, No. 6,
November-December 2021, pp. 1272-1280.
https://doi.org/10.2514/1.C036179.

Simplified Hybrid Laminar Flow Control on an A320 Fin. Retrofit Design and Sample Flight-Test Results

Geza Schrauf* and Heiko von Geyr†
DLR Institute of Aerodynamics and Flow Technology, 38108 Braunschweig, Germany

A flight test with a simplified Hybrid Laminar Flow Control (HLFC) system on the vertical tail plane (VTP) of an A320 aircraft was performed in April/May 2018. This HLFC system was a prototype for a simplified system that might be attractive for drag reduction of commercial long-range aircraft. The paper presents the design principles of a simplified HLFC system, including passive suction, and shows their application to aerodynamic and suction system design for the retrofit of an A320 VTP. Furthermore, sample flight test results will be presented and discussed.

I. Nomenclature

A	=	Cross-section area of throttle orifice, m^2
c_p	=	Pressure coefficient
c_q	=	w_s/v_∞, suction coefficient
C	=	Discharge coefficient of throttle orifice
p	=	Pressure, Pa
w_s	=	Averaged suction velocity, m/s
i_H	=	Setting angle of the horizontal tail plane, degree
H	=	Flight altitude, ft
M	=	Mach number
Re	=	Reynolds number
Re_{rr}	=	Roughness Reynolds number defined in [1]
β	=	Side slip angle, degree
δ	=	Rudder deflection angle, degree
η	=	Non-dimensional spanwise coordinate

Presented as Paper 2020-1536 at the AIAA SciTech Forum, 6-10 January 2020, Orlando, FL, USA.
*Research Scientist, DLR Institute of Aerodynamics and Flow Technology, Lilienthalplatz 7, 38108 Braunschweig, Germany, AIAA Senior Member.
†Head of Department, DLR Institute of Aerodynamics and Flow Technology, Lilienthalplatz 7, 38108 Braunschweig, Germany.

γ = Ratio of specific heats

μ = Viscosity, $kg(m * s)$

ρ = Density, kg/m^3

Subscripts:

q_c = Subscript ‘c’ denotes a quantity in a suction chamber

q_d = Subscript ‘d’ denotes a quantity in the plenum or duct

q_s = Subscript ‘s’ denotes a quantity on the outer side of the microperforation

q_0 = Subscript ‘0’ denotes a reference quantity

q_∞ = Subscript ‘∞’ denotes a quantity in the oncoming freestream

II. Introduction

Friction drag can constitute up to half of the total drag of an aircraft in cruise [2]. Laminar flow has the potential to significantly reduce friction drag, and thus, the fuel burn of transport aircraft. While smaller aircraft can achieve natural laminar flow (NLF) with suitable profile shaping, large aircraft require active boundary layer control by suction. For those aircraft, laminarity can be obtained by suction before the front spar in combination with a suitable shape of the wing box. This concept is called hybrid laminar flow control (HLFC). In spite of the potential of HLFC technology to lower fuel burn, work on the topic was largely neglected in Europe between 2003 and 2010. Airplane fuel was simply too cheap to make fuel burn reduction a priority, and only little research was published regarding the practical application of HLFC technology on large aircraft during this time. With increasing concern over climate change, however, attitudes changed and promoting laminar technology on commercial aircraft became interesting again.

The applicability of hybrid laminar flow control (HLFC) systems had already been shown in the 1990s by flying with such a system, for example, on the wing of a Boeing 757 [1] and, later, on the vertical tail plane (VTP) of an A320 [3, Fig. 1]. A good overview of the technology status of that time, can be found in [4]. However, the early suction systems using auxiliary compressors were very complex, heavy, and difficult to manufacture, and airlines remained hesitant to apply such HLFC systems in service. Clearly, the systems needed to be simpler, lighter and easier to produce, so that the benefit of drag reduction would not be canceled out by excessive weight, manufacturing costs or additional operational procedures. Industrial work using simplified systems including passive suction systems was done within the U.S. [5] and in Europe [6], however, not much has been published. This makes the present paper unique in its detailed description of our procedures and steps towards solving some of the practical problems arising in the implementation of HLFC systems.

In this paper, we principally explain the lighter, less complex HLFC system with which we have retrofitted the

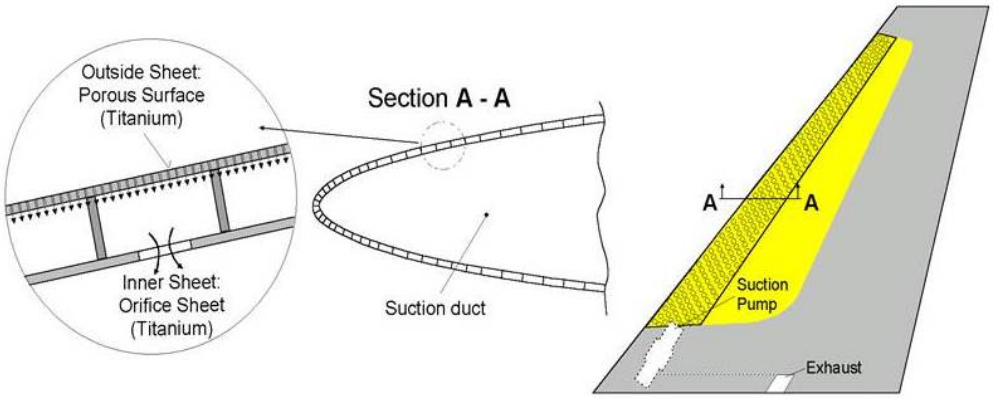

Fig. 1 Sketch of the simplified ALTTA system.

vertical tail-plane (VTP) of an A320 aircraft. Compared to a wing application, the VTP has the advantage that the HLFC-system integration is less complex. Furthermore, the aerodynamic shape of the baseline A320 VTP allows laminarity to mid-chord with an HLFC leading edge, enabling a systematic analysis of the HLFC-parameters. In our design work, the aerodynamic shape of the VTP remained unchanged.

III. Simplified ALTTA system

A major step towards simplification was the "simplified suction system," already proposed by Horstmann and Schröder [7] in 2001 within the European ALTTA project and also presented in [2]. A sketch of this system is shown in Fig. 1. They replaced the complex suction system used in previous aerodynamic feasibility flight tests by a simple double skin structure. The outer skin is, as before, a microperforated titanium sheet which is supported by an inner sheet with stringers. According to Horstmann, the small compartments created by the stringers should also act as suction chambers. This can be achieved with the help of throttle orifices. Thus, a complex system consisting of suction chambers, tubes, and valves is no longer necessary and can be replaced by an empty space: the plenum or suction duct. The challenge of this concept is that we no longer have the option to control the suction with the help of valves. The microperforation, the stringer locations, and the throttle holes must be balanced so that sufficient suction is generated for all flight conditions. In 2001, we could only show theoretical feasibility with numerical tools.

Much later, we were able to refine this concept as explained in Schrauf and von Geyr [3] and to build a full-scale wind-tunnel model of an A320 VTP as presented in Fig. 2. In 2014, we could finally test this model in the Large Low-Speed Facility (DNW-LLF) in the Netherlands. These tests at realistic flight Reynolds numbers (but at lower Mach number) proved that simplified HLFC is not only theoretically possible, but can be realized in practice.

The next logical step was to aim for a flight test demonstration. The aerodynamic and system design of the flight test article will be decribed in this paper.

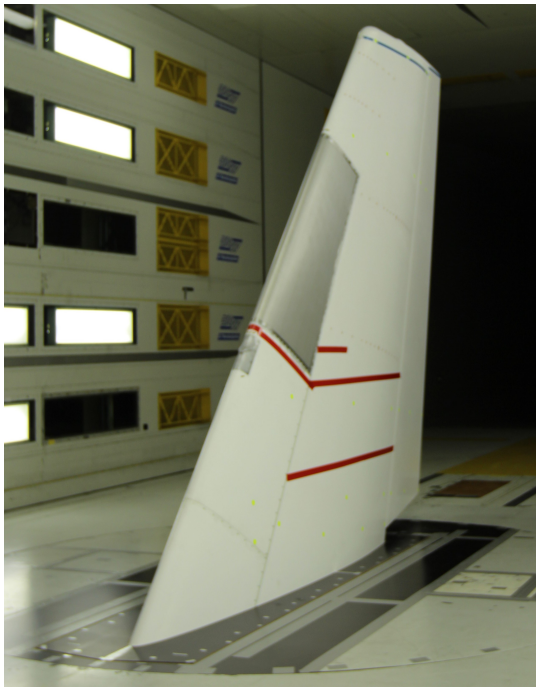

Fig. 2 Full-scale model of A320 VTP with refined simplified HLFC system in the DNW-LLF tunnel.

IV. Design of the Simplified HLFC System for the A320 VTP

The simplified suction system for the flying article was of the ALTTA type, i.e. it contained a microperforated outer sheet which was supported by an inner sheet with the help of stringers. The stringers form small chambers or compartments inside of the microperforation. The sucked-in air is discharged into a plenum through throttle orifices in the inner skin. The art of the design is to match the microperforation with stringer distances, throttle hole size and number of throttle holes, so that sufficient suction is generated to suppress cross-flow transition for all relevant cruise flight conditions.

For this flight test, the suction system had to run in two modes, an active mode, driven by a pump, and a passive mode, in which suction was generated with the help of a flap. The design range for the active mode is given in Table 1. For the passive mode, we relaxed the requirements for side slip and rudder angles to only ±1 degree. Due to the

Table 1 Design range for the HLFC system.

Flight altitude	H	$29000ft$, $31000ft$, ..., $39000ft$
Mach number	M	0.76, 0.78, 0.80
Side slip angle	β	-2^0, -1^0, 0^0, 1^0, 2^0
Rudder deflection angle	δ	-2^0, -1^0, 0^0, 1^0, 2^0

symmetry of the VTP, we did not need to consider all possible combinations of the angles β and δ. It was sufficient to perform design calculations for the cases ($\beta = 0^0, \delta = 0^0$), ($1^0, -1^0$) and ($2^0, -2^0$)*. For structural design, the case

*The combination of positive side slip angle and negative rudder deflection angle produces the largest flow deflection. Alternatively, one could use opposite signs.

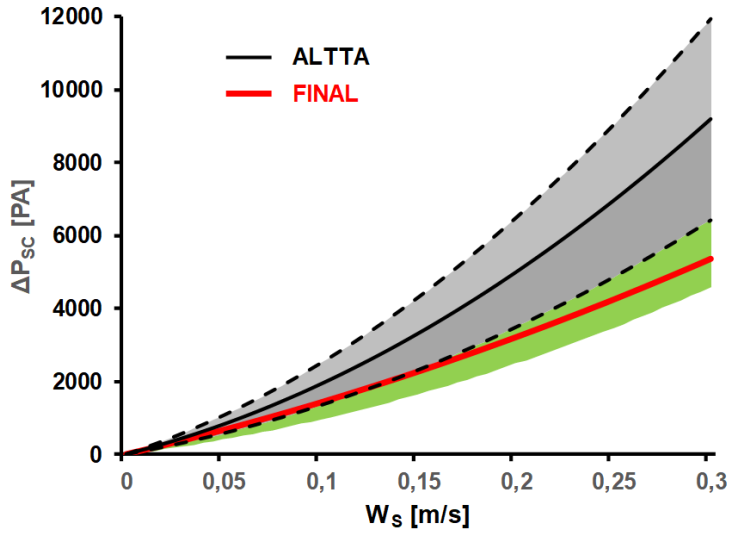

Fig. 3 Design range of pressure loss characteristics.

$H = 29000\,ft$, $M = 0.8$, $\beta = 2^0$ and $\delta = -2^0$ is the most critical one regarding pressure loads.

A. Microperforation Specification Development

We simplified the design task by separating aerodynamic and system design from the manufacturing of the suction panel. This means that we do not consider any geometric properties of the microperforation, such as diameter, conicity, or pitch of the suction holes. However, we do assume that the microperforation can be described by a pressure-loss characteristic of the form[†]

$$\Delta p \;=\; A\,\frac{\mu_s}{\mu_0}\,w_s \;+\; B\,\frac{\rho_s}{\rho_0}\,w_s^2. \tag{1}$$

The initial values for the coefficients, $A = 13553\,kg/(m^2\,s)$ and $B = 56845\,kg\,s/m^3$, were taken from the ALTTA project [7]. We did not consider a single characteristic, but allowed for the gray range shown in Fig. 3. With this, we could work on the aerodynamic as well as on the system design of the HLFC system, requiring that the design should work for each pressure-loss characteristic within this range. In parallel, the producer of the microperforated panel began developing a stable manufacturing process, which would guarantee that the pressure-loss characteristic of the manufactured panel was within the same range. This task, however, was more difficult than anticipated, even with today's modern laser-drilling capabilities. The development of a stable process took several years, and the pressure-loss characteristic which could be reliably obtained was still slightly outside of the design range. Meanwhile, it had become clear that pressure-drop tolerance requirements for the A320 VTP microperforation were less stringent than originally thought. We found that we could expand the design range by including the green area with no adverse effect.

During the process development, several test samples were produced and their pressure-loss charactistics were

[†]The reference quantities are the values of the standard atmosphere at sea level, i.e. $\mu_0 = 1.792\,10^{-5}\,kg/(m\,s)$, and $\rho_0 = 1.225\,kg/m^3$.

measured with a laminar flow meter [8]. The pressure-loss characteristic of the final suction sheet was measured by using test pieces made from left over material. Finally, after the assembly of the HLFC leading edge, the microperforation pressure-drop characteristics were again checked with a portable flow meter developed for this purpose.

B. Details of the Suction Sheet

The suction sheet is made out of titanium with a thickness of $0.8mm$. The final values of the diameters of the suction holes are in the order of $55\mu m$ and the average hole distance is $565\mu m$. The final pressure-loss characteristic is shown as a red line in Fig. 3. The values of its pressure-loss coefficients are $A = 12400\,kg/(m^2\,s)$ and $B = 18270\,kg\,s/m^3$.

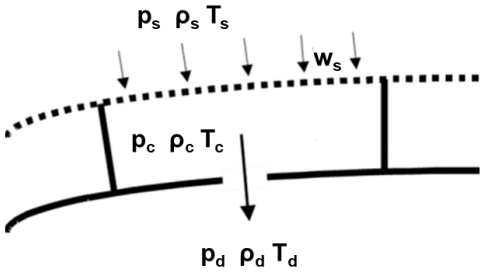

Fig. 4 Suction chamber and inner panel with a throttle hole.

C. Throttle Holes

The stringers and the inner sheet with the throttle orifices are also manufactured out of $0.8mm$ thick titanium plates. The inner sheet has throttle holes, as shown in Fig. 4, to generate sufficient suction in each small chamber and for each flight condition. We can determine the size and the number of throttle holes for each suction chamber with the help of the equation

$$\dot{m} = C\ A\ \sqrt{p_c\,\rho_c\,\frac{2\gamma}{\gamma-1}\left\{\left(\frac{p_d}{p_c}\right)^{2/\gamma} - \left(\frac{p_d}{p_c}\right)^{(\gamma+1)/\gamma}\right\}} \tag{2}$$

for the mass flow through one throttle orifice with cross section area A. This equation is an extension of the compressible Bernoulli equation [3, 9]. Herein, C is the discharge coefficient of the throttle orifice. As before, specimens with throttle holes of different sizes were drilled and their discharge coefficients were determined with the flow meter[‡]. It is a good practice to avoid throttle holes which are too small. Their discharge coefficients might exhibit large variations induced by small geometric irregularities of their edges. With larger holes, the influence of the edges is weaker. This is because the circumference of a hole increases linearly with the diameter, whereas its area increases quadratically, so that the ratio "circumference/area" becomes smaller.

The mass flow through one chamber can be computed with equations (1) and (2). The equations for all chambers

[‡]Flache, B., and Seitz, A., "Discharge coefficients of orifice plates," private communication, 2016. Results for holes in carbon fibre reinforced plastics (CFRP) are published in [10].

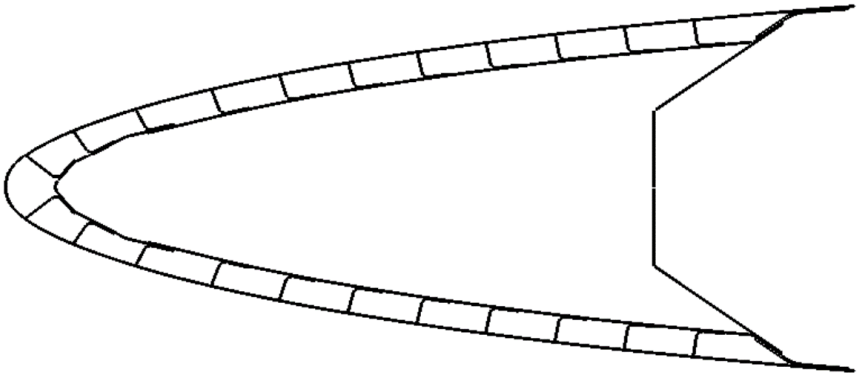

Fig. 5 Suction chamber layout of the HLFC leading edge.

form a system with a special structure which can be solved with a fast algorithm [11]. This algorithm is implemented in the program SCDP [12], with which we calculated the suction velocities as input for the boundary layer computations.

D. Aerodynamic Chamber Design

The stringers between the microperforated outer skin and the inner sheet with the throttle holes have two functions: first, to provide structural stiffness and strength, and, second, to form small suction chambers. A sketch of this double skin is shown in Fig. 5. From the aerodynamic point of view, we have the following requirements on the stringer positions and on the microperforation:

1) Keep the attachment line laminar by satisfying the K-criterion [13]
2) No stringer should be positioned at the leading edge to allow for suction at the attachment line
3) Generate sufficient suction to delay transition
4) Allow for local blockage caused by the stringer weld lines
5) Avoid outflow when flying with sideslip, because outflow triggers immediate transition
6) Avoid transition by "equivalent roughness," aim for Re_{rr} values below $400 - 450$ (cf. [1])
7) Avoid choking in the suction holes by keeping the Mach number of the hole flow below 0.3
8) Minimize mass flow and suction power
9) Aim for a robust design by allowing for a large variation of the pressure-loss characteristic of the microperforation

In the above list,requirements 1-5 are strict, meaning that if one of them is violated,laminarity is lost. Items 6 and 7 are good design guidelines, but these values can be relaxed.

To carry out the chamber design, we used the following numerical tools:

- 3D-RANS computations for the complete A320 configuration with the DLR-TAU code [14, 15]
- Grid generation with SOLAR [16] using 81 million nodes
- Rudder deflection and HTP trim setting realized by grid deformation
- Suction velocities, stringer positions, and chamber flow calculated with SCDP [12]
- Boundary layer and stability calculations by COCO [17] and LILO [18]

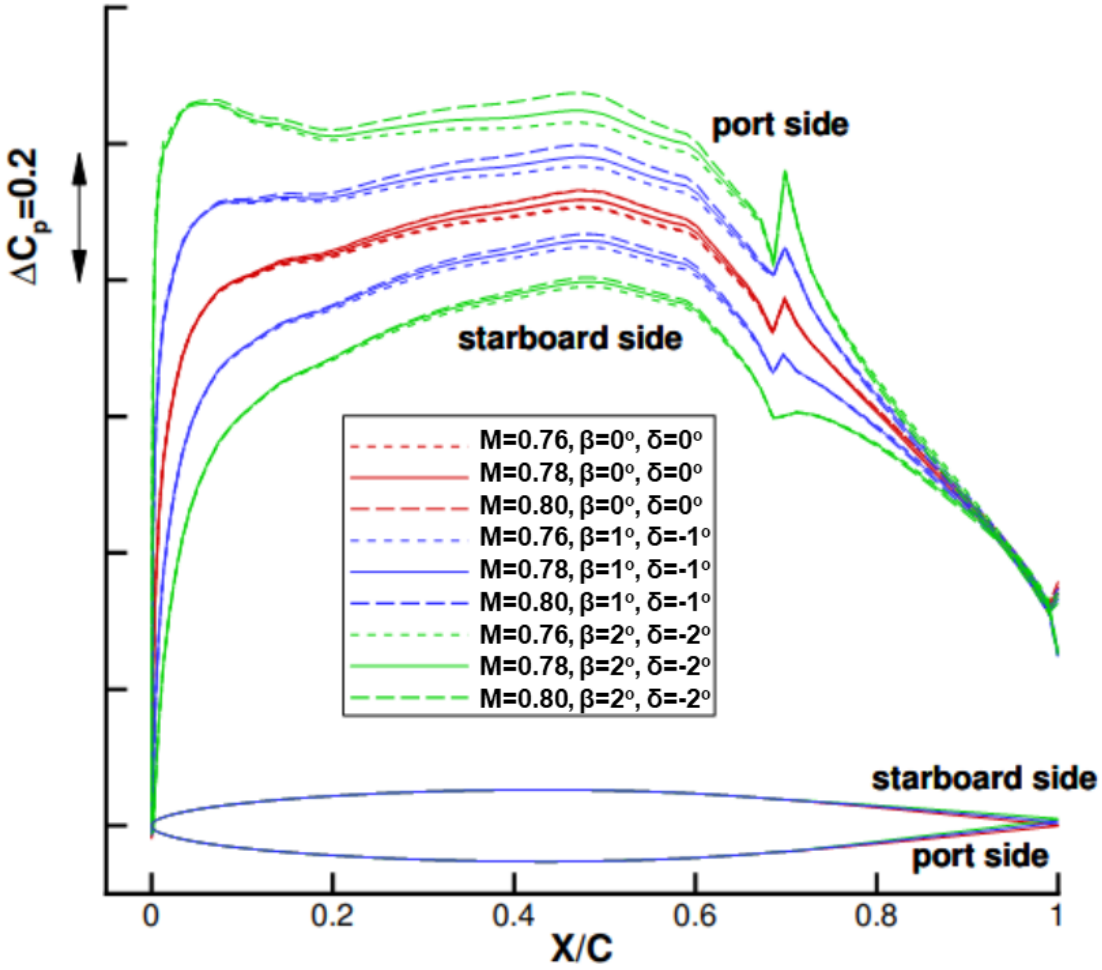

Fig. 6 Pressure distributions at $\eta = 56\%$ of VTP, $H = 31000\,ft$.

E. Details of Design

Next, we present key results from the HLFC design cycles. Fig. 6 shows pressure distributions for flight altitude 31000 ft, Mach numbers 0.76, 0.78, and 0.80, sideslip angles changing from 0^0 to 2^0, as well as rudder deflection angles 0^0, -1^0, and -2^0. We see that all pressure distributions have large gradients at the leading edge, limiting the size

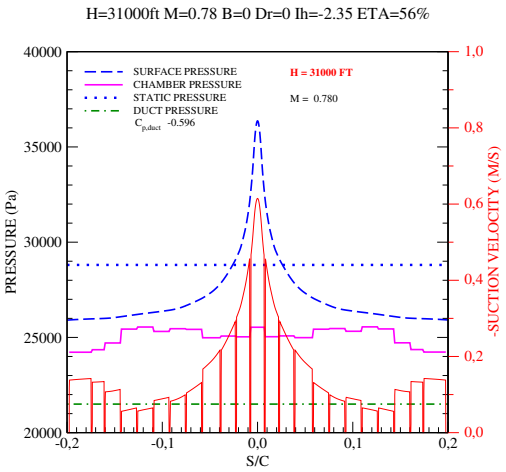

(a) Surface pressure, system pressures, and suction velocities.

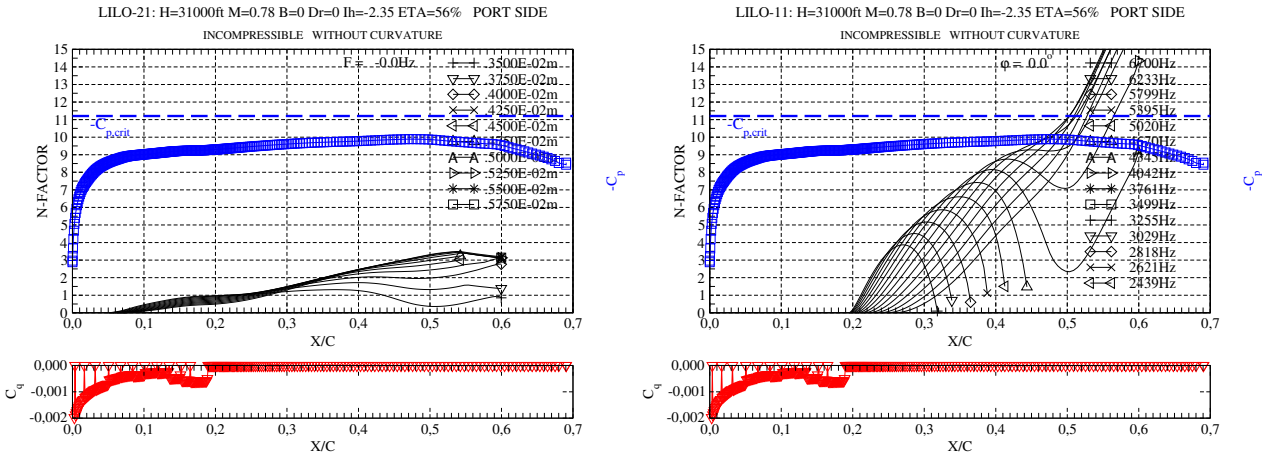

(b) N_{CF}-factors for the port side.

(c) N_{TS}-factors for the port side.

Fig. 7 System pressures and N-factors for a symmetric case.

of the suction chambers in this region. Away from the leading edge, i.e. for $X/C > 0.05$, the pressure gradients are much smaller, so that from the aerodynamic point of view, only a few large chambers would be needed. Here structural requirements are driving the number and the positions of the stringers. Fig. 5 shows the final layout with twenty-three suction chambers.

In Fig. 7a we present some results for a symmetric case with flight altitude $31000\,ft$, Mach number 0.78, and sideslip angle as well as rudder deflection angle 0^o. The pressure along the outer surface is shown with the blue curve and the chamber pressures with the piecewise constant, pink one. Furthermore, we have, in red, the suction velocities generated by this pressure difference. We see that the suction velocity between two chambers is zero, due to the blockage at the weld line. The horizontal green line represents the plenum or duct pressure, which, in this calculation, is $21500Pa$.

The N_{CF}- and N_{TS}-factors are shown in Figs. 7b and 7c. As expected, suction limits the growth of the N_{CF}-factors and delays TS-growth until the end of the suction panel. Downstream of it, we observe strong growth of Tollmien-

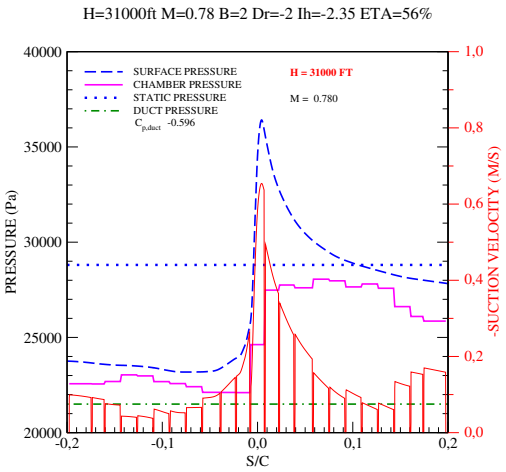

(a) Surface pressure, system pressures, and suction velocities.

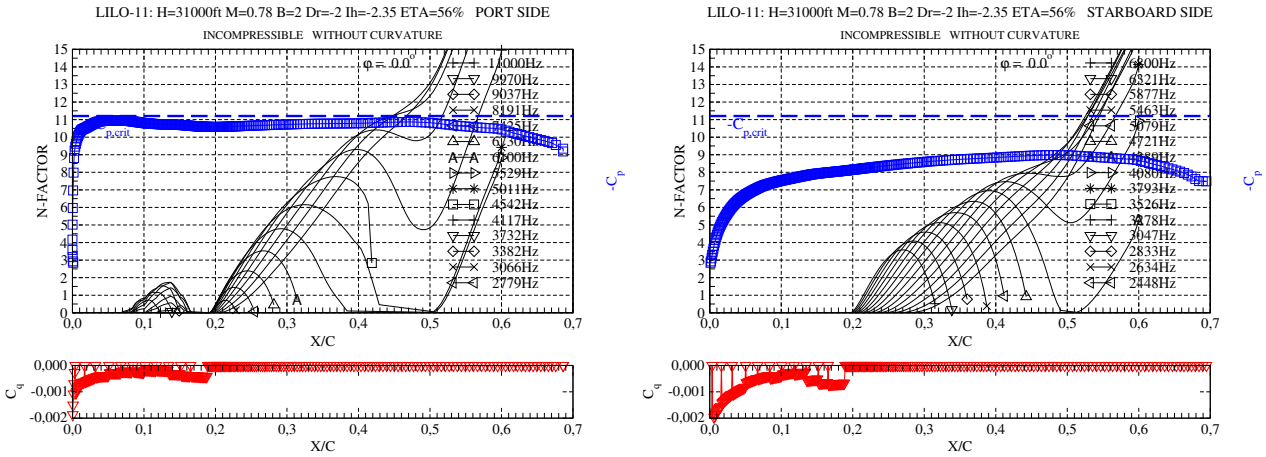

(b) N_{TS}-factors for port side.

(c) N_{TS}-factors for starboard side.

Fig. 8 System pressures and N-factors for an asymmetric case with two degrees sideslip.

Schlichting waves leading to transition. Assuming a critical N_{TS}-factor of 9.5, we predict transition to occur at 43% chord.

In Fig. 8 we present a case at the same flight altitude, Mach number, and plenum pressure, however, this time with sideslip angle 2^o and rudder deflection angle of -2^o. This asymmetry is reflected in the pressure distribution (cf. Fig. 8a). We see that the difference between inside and outside pressure becomes very small at the port (left) side of the nose chamber around $S/C = -0.007$. A further increase of the plenum pressure or an enlargement of the nose chamber would cause flow reversal at this location, i.e. air would leave the suction chamber through the microperforation. This local outflow[§] would cause the boundary layer to become turbulent. By reducing the sideslip angle, the pressure distribution becomes less asymmetrical as can be seen from Fig. 6. Thus, the difference between inside and outside pressure at $S/C = -0.007$ becomes larger, so that suction is still achieved for higher plenum pressures which can be

[§]We distinguish between local and global outflow. With local outflow, there is still suction over some parts of the chamber, whereas global outlow means outflow over the whole chamber.

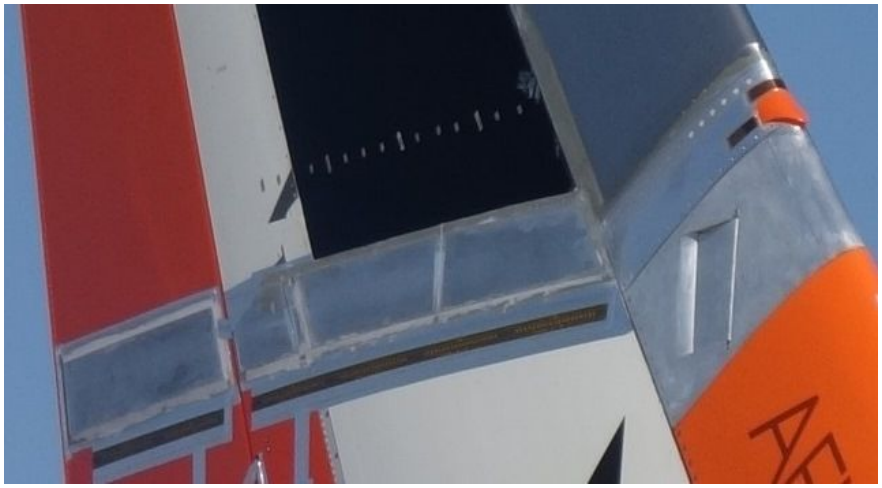

Fig. 9 Suction flap on starboard side of the A320 ATRA aircraft.

generated with less power. This is why we relaxed the design requirements for passive suction: the suction power of a flap might be more limited than that of a pump.

In Fig. 8b and 8c we present the N_{TS}-factors for both sides. We do not show the N_{CF}-factors because they are small. On both sides, transition is caused by Tollmien-Schlichting instability, at 38% chord on the port side and at starboard to 42% chord[¶]. We also observe a local region with weak growth of Tollmien-Schlichting waves at $X/C = 0.1$ on the port side in the region of adverse pressure gradient (Fig. 8b), resulting from the weaker suction at this location.

V. Flight Test Instrumentation and Installation

As mentioned before, the suction power for the HLFC system was to be generated in two ways. First, in an active mode, in which suction was generated with the help of an array of small, off-the-shelf pumps that were already certified for flight. In the second or passive mode, suction was generated with a flap (actuated ramp with aft-facing opening) on the starboard side, shown in Fig. 9, which could be opened and closed from the cabin.

The functionality of the suction system was verified with the following multitude of sensors (see Fig. 10):

- In each suction chamber with two pneumatic pressure probes connected to pressure transducers and with two MEMS sensors measuring temperature, pressure, and humidity, one at 25% and the other one at 75% span of the suction panel (cf. Fig. 10)
- In the plenum or duct with two pneumatic pressure probes and with two MEMS sensors measuring temperature, pressure, and humidity one at 25% and the other at 75% span
- Two sections with pneumatic surface pressure orifices, DV1 at 39% span and DV2 at 67% span of the VTP (cf. Fig. 10)

[¶]On the starboard side, the assumed critical N_{TS}-factor is somewhat lower than on the port side to account for larger crossflow amplification. The critical N-factors used for design are shown in [19].

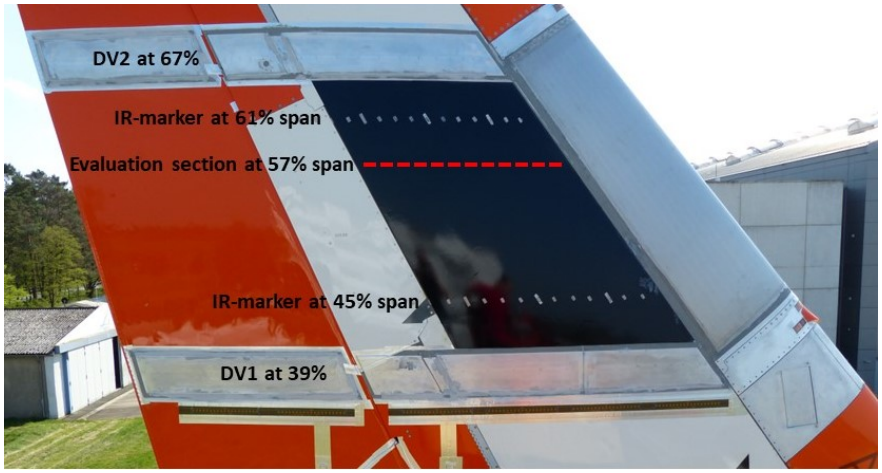

Fig. 10 Pressure sections DV1 and DV2 on starboard side.

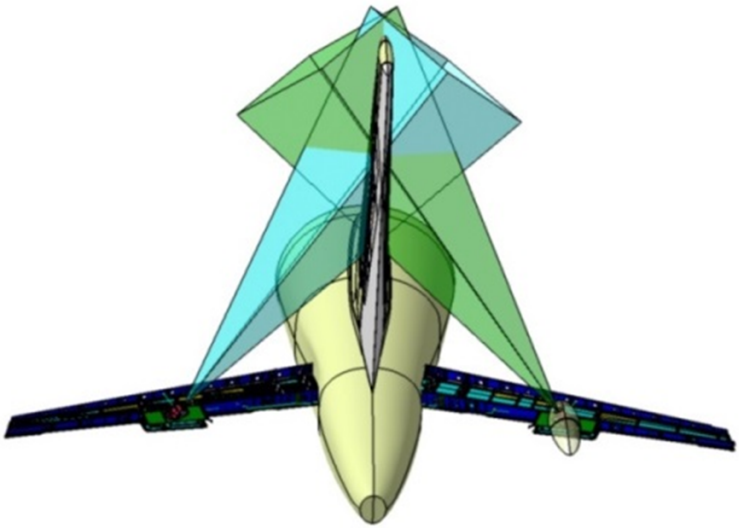

Fig. 11 Infrared cameras mounted in the horizontal tail planes.

- Additionally, a MEMS pressure belt on each side of the VTP box below DV1
- A mass flow meter before the pump, for active suction only
- Two infrared cameras for simultanous transition detection on both sides of the VTP, installed in the horizontal tail plane and covered with fairings (cf. Fig. 11)
- Hot film sensors to check the laminarity of the flow at the attachment line

In contrast to earlier HLFC flight test from 1998 with a different and much more complex suction system [20, 21], we did not install a heater mat for the visualization of the laminar-turbulent transition with infra-red thermography. This time we relied on sun heating of the black foil shown in Figure 10 and found this to be sufficient.

Fig. 12 DLR A320 ATRA aircraft with HLFC system installed in the VTP.

Finally, Fig. 12 shows the aircraft with the installed HLFC segment on the VTP on the tarmac at Brunswick airport.

VI. Sample Flight Test Results

We present two flight measurements. In the first one, measurement A, the aircraft was flying at Mach number 0.78 at altitude of $35000\,ft$. At the time the infrared image in Fig. 13a was taken, the sideslip angle was β was -0.2^o and the rudder deflection angle -0.7^o, so that we can consider this case to be nearly symmetric. The infrared image shows good contrast, because this side of the VTP was illuminated by the sun. The result of the image processing is shown in Fig. 13b with the green line indicating transition, which occurs between 36.5% and 38% chord in the spanwise range $0.56 < \eta < 0.59$. The transition line was obtained by an automated image processing and analysis tool to avoid possible human bias associated with manual transition-line determinations.

The two plenum pressures at 25% and 75% span were 17061 Pa and 17086 Pa, respectively, so that the spanwise pressure difference is only 25 Pa or 0.15%. With the freestream pressure $p_\infty = 23840\,Pa$, we obtain a difference between the averaged plenum pressure and the freestream pressure of 6766 Pa, i.e. we have a case with strong active suction. The relative humidity of the air in the plenum was 5%, that is, the air was very dry.

In Figures 13c and 13d, we present the results of boundary layer and subsequent stability analysis with incompressible[‖] theory, performed at the spanwise section of 57%. Because of the strong suction, crossflow and Tollmien-Schlichting instabilities are completely damped over the suction panel. Further downstream, on the VTP box, we observe weak CF and strong TS amplification which then triggers transition. With a measured transition location of $0.365 < X/C < 0.38$, we obtain a correlated transition N_{TS}-factor between 8.5 and 8.8.

Next, we present flight test measurement B, which was also taken at flight altitude $35000\,ft$ and Mach number 0.78. Sideslip and rudder deflection angles were 0.1^o and -0.4^o, respectively, i.e. we again have a symmetric case. This time, the starboard side was the shady side, so that the contrast in the infrared image is less pronounced. According to the

[‖] For transonic flow, we prefer N-factors computed with incompressible stability theory, because the N-factors obtained with compressible stability theory exhibit a larger Mach number dependence as shown in Atkin and Schrauf [22, Fig. 9]. The correlated compressible N_{TS}-factor would be on the order of 5.

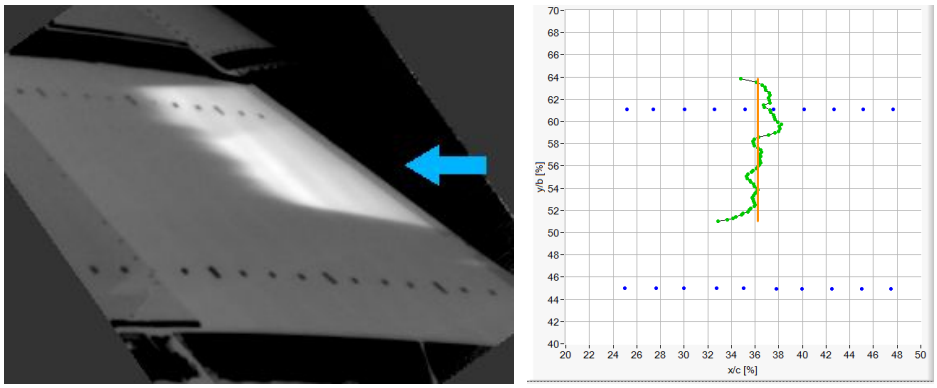

(a) Infrared image of starboard side.

(b) Transition line.

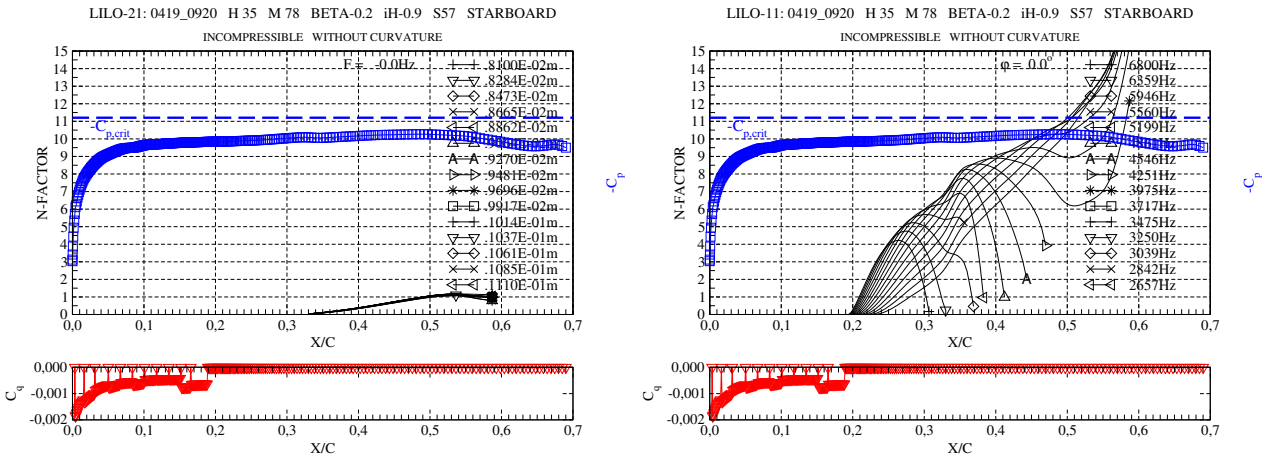

(c) N_{CF}-factors.

(d) N_{TS}-factors.

Fig. 13 Flight test measurement A.

image processing shown in Fig. 14b, transition occurred between 48% and 50% in the spanwise range $0.56 < \eta < 0.59$. The plenum pressures were 19649 Pa and 19654 Pa. The difference between averaged plenum and freestream pressure was only 3613 Pa, i.e. much smaller than for the previous measurement. The effect of the weaker suction can be seen in Fig. 14c, showing some CF amplification** over the suction panel. Nevertheless, transition is still triggered by the Tollmien-Schlichting instability. The correlated N_{TS}-factors are 10.0 – 10.5. They are somewhat larger than for measurement A.

This might result from a moderately lower surface temperature because, for this measurement, the starboard side was the shady side and it is known that surface heating provokes an earlier transition [23, 24]. Whether this is a systematic temperature effect needs to be further investigated.

**Without suction, transition would be caused by the cross-flow instability very close to the leading edge, as is demonstrated in [3, Fig. 13].

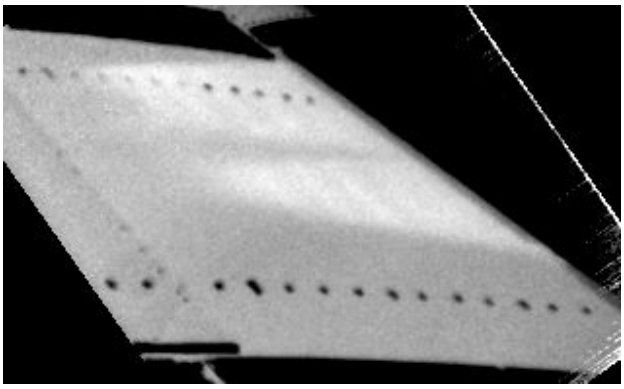

(a) Infrared image of starboard side.

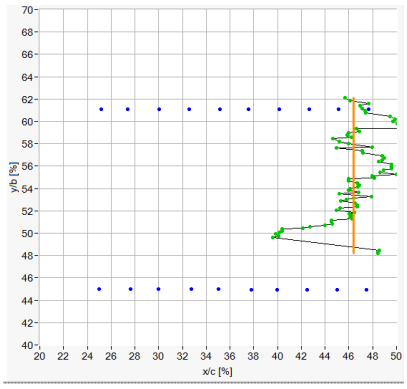

(b) Transition line.

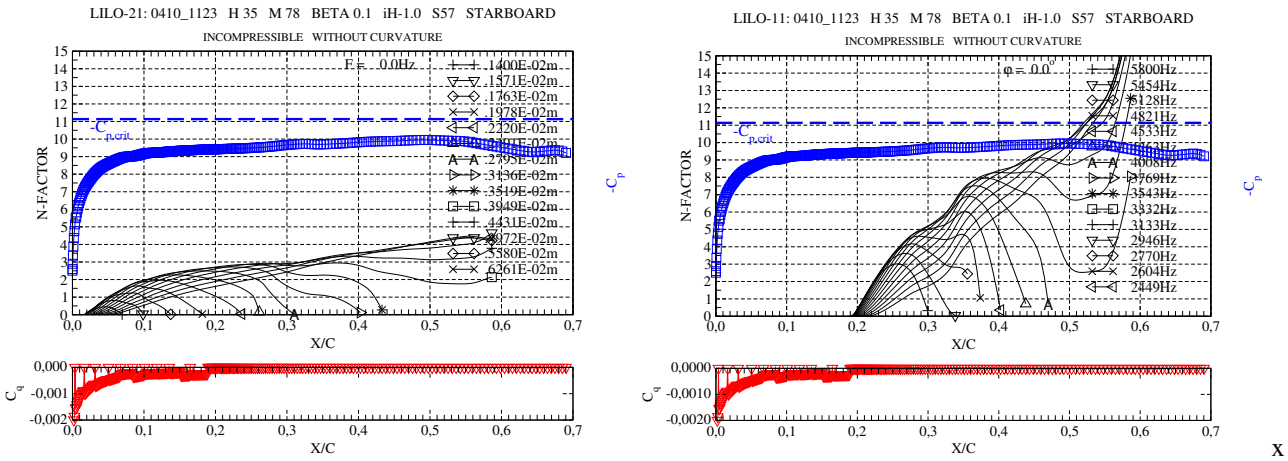

(c) N_{CF}-factors.

(d) N_{TS}-factors.

Fig. 14 Flight test measurement B.

VII. Remarks on Main HLFC Challenges

Before closing, a summary of the main challenges for the application of HLFC to commercial aircraft would be appropriate. They are:

A Minimizing complexity of the system, weight, and manufacturing cost

B Maintaining the smoothness of the laminar-flow surface over the lifetime of the aircraft

C Understanding of operational issues, such as de- or anti-icing, insect contamination,ice clouds, ...

The first point (A) is the topic of this paper and needs no further space. As for maintaining the smoothness of the surface over the lifetime of the aircraft (B), we have solutions to maintaining a good surface quality of a joint, such as, for example [25]. These solutions can be applied for HLFC segments, such as the leading edge of a VTP, which need no or only very few replacements during the lifetime of the aircraft. For a wing leading edge, the situation is more complex. Because wings can be damaged on the tarmac by ground vehicles, a wing leading edge is more likely to need replacement. A concept for such a detachable leading edge consistent with the aero-smoothness requirements was developed for the natural-laminar-flow BLADE wing [26, 27].

Some leading edges of aerodynamic surfaces need de- or anti-icing. It has been shown that leading-edge suction can be made compatible with de- or anti-icing needs [28–31]. The loss of laminarity due to insect contamination has been investigated (see, for example [32]), and can be estimated using insect density profiles [33, 34] for take-off and landing. Insect contamination is mostly a problem for airports in warm and humid climates. For the affected routes, the increase in fuel burn needs to be taken into account [35]. However, for many other city pairs the impact is less severe, and flying through rain after take-off will clean the leading edges. Flying through ice clouds is also detrimental to laminarity and must be factored into the overall balance when calculating the benefits of HLFC [36].

VIII. Conclusions

In this paper we have presented the design of a simplified suction system to achieve laminar flow on the vertical tail plane of an A320 aircraft. We have explained the design requirements, which are also valid for simplified HLFC systems in horizontal tail planes as well as for wings, paying attention to the sizing of the suction chambers in view of the outer pressure distribution and the micro-perforation. Furthermore, we have shown how to allow for perforation-skin manufacturing deviations by prescribing a design range for the pressure loss characteristics of the suction panel. Finally, we described the comprehensive flight-test measuring system, including the infra-red thermography for transition detection which worked without a heater mat. To demonstrate the validity of the design, we presented two sample flight-test measurements during which the aircraft flew without sideslip. We found that the correlated N_{TS}-factors, obtained with incompressible stability theory, are in the expected range. Furthermore, we observed a possible effect of the surface temperature (due to solar heating on the dark test surface) on Tollmien-Schlichting transition.

Acknowledgments

The flight test activities received funding from the European Community's Seventh Framework Programme FP7/2007-2013, under grant agreement n° 604013, AFLoNext project. The activities were performed within AFLoNext Workpackage 1.1 with support of the partner Airbus Operations GmbH, Airbus Operations S.A.S, Airbus Operations SL, Dassault Aviation SA, SONACA, TAI, AcQ Inducom, IBK Innovation, CIRA, DLR, FOI, Fraunhofer, and ONERA.

Special thanks to Philipp Mühlmann (DLR, German Aerospace Center) for processing the IR-images, to Klaus de Groot (DLR, German Aerospace Center) for providing the flight test data, and to Nancy Schrauf for editing.

References

[1] Boeing Commercial Aircraft Group, "High Reynolds Number Hybrid Laminar Flow Control (HLFC) Flight Experiment II. Aerodynamic Design," NASA CR-1999-209324, April 1999.

[2] Schrauf, G., "Status and Perspective of Laminar Flow," *The Aeronautical Journal*, Vol. 109, No. 1102, 2005, pp. 639–644. https://doi.org/10.1017/s000192400000097x.

[3] Schrauf, G., and von Geyr, H., "Simplified Hybrid Laminar Flow Control for Transport Aircraft." In Eberhardsteiner J. et al. (eds), *European Congress on Computational Methods in Applied Sciences and Engineering (ECCOMAS 2012)*, 2012, Vienna, Austria.

[4] Braslow, A. L., "A History of Suction-Type Laminar-Flow Control with Emphasis in Flight Reserach," *Monographs in Aerospace History*, No.13, NASA History Division, 1999, Washington, DC.

[5] Kingsley-Jones, M., "FARNBOROUGH: Aero secrets of Boeing's new Dreamliner," FlightGlobal, 18 July 2014, `https://www.flightglobal.com/farnborough-aero-secrets-of-boeings-new-dreamliner/113955.article`.

[6] Dubois, Th., "EU Reserach Sets Sights on Laminar Flow for Drag Reduction," Aviation Week & Space Technology, February 25, 2019 - March 10, 2019, p. 47.

[7] Horstmann, K. H., and Schröder, W., "A Simplified Suction System for a HLFC L/E Box of an A320 Fin," *ALTTA Technical Report*, No. 23, 2001.

[8] Seitz, A., "Messkörper, Durchflussmesssystem und Computerprogramm dafür," Offenlegungsschrift DE 2015 113 999 A1 2016.03.03, Anmeldetag 24.08.2015, Offenlegungstag 03.03.2016, Deutsches Patent- und Markenamt.

[9] Idelchik, I. E., "Handbook of Hydraulic Resistance," Jaico Publishing House, Mumbai, 2003. English Translation from the second Russian edition, 1975.

[10] Kilian, T., Forßbohm, T., Seitz, A. and Flache, B., "Discharge characteristics of drilled throttle orifices in fiber-reinforced plastics for an HLFC system," CEAS Aeronautical Journal, Vol. 11, 2020, 431–439. https://doi.org/10.1007/s13272-019-00416-y.

[11] Keller, H. B., "Numerical Solutions of Bifurcation and Non-Linear Eigenvalue Problems." In Rabinowitz P. (ed.), *Application of Bifurcation Theory*. Academic Press, New York, 1977, pp. 359 -384.

[12] Schrauf, G. "SCDP – A Suction Chamber Design Program. Version 1.5," *GSSC Technical Report* No. 8.5, January 2015.

[13] Arnal, D., Juillien, J. C., Reneaux, J., and Gasparian, G., "Effect of Wall Suction on Leading Edge Contamination," *Aerospace Science and Technology*, No. 8, 1997, pp 505-571. https://doi.org/10.1016/s1270-9638%2897%2990000-6 .

[14] "TAU-Code User Guide," Release 2007.1.0, Institute of Aerodynamics and Flow Technology, German Aerospace Center, April 2007.

[15] Schwamborn, D., Gerhold, T., and Heinrich, R., "The DLR TAU-Code: Recent Applications in Research and Industry," In: Wesseling P., Oñate E., and Périaux J. (eds.), *European Conference on Computational Fluid Dynamics, ECCOMAS CFD 2006*, Egmond aan Zee, The Netherlands, 5-8 September 2006, CD-Rom Proceedings, ISBN: 90-9020970-0, TU Delft,The Netherlands.

[16] Martineau, D., Stokes, S., Munday, S., Jackson, A., Gribben, B., and Verhoeven, N., "Anisotropic Hybrid Mesh Generation for Industrial RANS Applications. Collection of Technical Papers." 44th AIAA Aerospace Sciences Meeting, 9-12 January 2006, Reno, Nevada. doi:9.10.2514/6.2006-534.

[17] "COCO - A Program to Compute Velocity and Temperature Profiles for Local and Nonlocal Stability Analysis of Compressible, Conical Boundary Layers with Suction," *ZARM Technik Report*, November 1998.

[18] Schrauf, G., "LILO 2.1 User's Guide and Tutorial," Bremen, Germany, *GSSC Technical Report* No. 6, originally issued 2004, modified for Version 2.1 July 2006.

[19] Schrauf, G., and von Geyr, H., "Simplified Hybrid Laminar Flow Control for the A320 Fin. Part 2: Evaluation with the e^N-method." AIAA SciTech Forum, 11-15 & 19-21 January 2021, Virtual Event. https://doi.org/10.2514/6.2021-1305.

[20] Henke, R., ""A320 HLF Fin" Flight Tests Completed." Air&Space Europe, Vol 1, No.2, 1999, 76-79. https://doi.org/10.1016/s1290-0958(99)80019-7.

[21] Henke, R., "First Results from the A320 HLF Fin Programme." In: Nitsche W., Heinemann HJ., Hilbig R. (eds), "New Results in Numerical and Experimental Fluid Mechanics II. Notes on Numerical Fluid Mechanics (NNFM)," Vol 72., 1999, Vieweg+Teubner Verlag, Wiesbaden, pp. 234-241. https://doi.org/10.1016/s1290-0958(99)80019-7.

[22] Atkin, C., and Schrauf, G., "Progress in Linear Stability Methods for Design Applications," ECCOMAS 2000, 11-14 September 2000, Barcelona, Spain. CD-ROM Proceedings by ECCOMAS, ISBN: 84-89925-70-4. http://openaccess.city.ac.uk/14204/.

[23] Masad, J. A., and Malik, M. R., "Transition Correlation in Subsonic Flow over a Flat Plate." AIAA Journal, Vol 31, No.10, Oct 1993. https://doi.org/10.2514/3.11872.

[24] Stock, H.-W., "Wind tunnel-flight correlation for laminar wings in adiabatic and heating flow conditions." Aerospace Science and Technology, Vol. 6, (2002), 245-257. https://doi.org/10.1016/S1270-9638%2802%2901166-5.

[25] Parikh, P.G., Koppelman, H.J., Harris, T.M., and Swanstrom, F.M., "Skin panel joint for improved airflow," United States Patent 8,282,042, Document US 20100320325 A1, 9 October, 2012, The Boeing Company, Chicago, Il.

[26] Gubisch. M., "Airbus readies laminar-winged A340 for test flights," FlightGlobal, 4 September 2017, https://www.flightglobal.com/analysis-airbus-readies-laminar-winged-a340-for-test-flights/125260.article.

[27] Airbus, "Airbus 'BLADE' laminar flow wing demonstrator makes first," Airbus, 26.09.2017, https://www.airbus.com/newsroom/press-releases/en/2017/09/airbus_-_blade_-laminar-flow-wing-demonstrator-makes-first-fligh.html.

[28] Wagner, R.D., Maddalon, D.V., and Fisher, D.F., "Laminar Flow Control Leading Edge Systems in Simulated Airline Service," 16th Congress of the International Council of the Aeronautical Sciences, Jerusalem, Israel, August 28 - September 2, 1988. https://doi.org/10.2514/3.45925.

[29] Humphreys, B., Totland, E. , Young, T. , Corish J., and Whooley, A. , "In-service Test of Laminar Flow Materials and De-contamination System for Hybrid Laminar Flow Control," HYLTEC Technical Report TR 64, December 2001.

[30] Young, T., Mahony, B., Humphreys, B., Totland, E., McClafferty, A., and Corish, J., "Durability of Hybrid Laminar Flow Control (HLFC) Surfaces," Aerospace Science and Technology No. 7 (2003), pp. 181-190. https://doi.org/10.1016/s1270-9638%2803%2900013-0.

[31] Horstmann, K.H., and Meyer, J.B., "Flight Testing of Anti-Icing and Anti-Contamination Systems for HLFC Surfaces," KATnet Flow Control Workshop, Poitiers, France, 12.-13.10.2004.

[32] Elsenaar, A., and Haasnoot, H. N., "A survey on Schipol Airport of the Contamination of Wing Leading Edges of Three Different Aircraft Types under Operating Conditions." First European Forum on Laminar Flow Technology, Hamburg, Germany, March 16-18, 1992.

[33] Beerwinkle, K. R., Lopez, J. D., Schleider, P. G., and Lingren, P. D., "Annual patterns of aerial insect densities at altitudes from 500 to 2400 meters in east-central Texas indicated bay continuously-operating vertically-oriented radar," Society of Southwestern Entomologists, The Southwestern Entomologist, 1995, Supplement 18, pp. 63-79.

[34] Smith, A.D., Reynolds, R., and Riley, J.R., "The use of Vertical-Looking Radar to continuously monitor the insect fauna flying at altitude over southern England," Bulletin of Entomological Research 90(2000), pp. 265–277 https://doi.org/10.1017/S0007485300000389.

[35] Wicke, K., Linke, F., Gollnick, V., and Kruse, M., "Insect Contamination Impact on Operational and Economic Effectiveness of Natural-Laminar-Flow Aircraft," Journal of Aircraft, Vol. 53, No. 1, 2016, pp. 158-167. https://doi.org/10.2514/1.c033237.

[36] Pohya, A. A., Wicke, K., Risse, K., Linke F., Lau A., Lührs, B., and Swaid, M., "Cloud Encounter Impact on Operational and Economical Effectiveness of Hybrid-Laminar-Flow-Control Aircraft," Journal of Aircraft, Vol. 56, No. 4, 2019, pp. 1513-1523. https://doi.org/10.2514/1.c035205.